Science of the Total Environment xxx (xxxx) xxx

Contents lists available at ScienceDirect

Science of the Total Environment

journal homepage: www.elsevier.com/locate/scitotenv

Variations of sedimentary Fe and Mn fractions under changing lake mixing regimes, oxygenation and land surface processes during Late-glacial and Holocene times

Stamatina Makri [a,*], Giulia Wienhues [a], Moritz Bigalke [a], Adrian Gilli [b], Fabian Rey [c], Willy Tinner [c], Hendrik Vogel [d], Martin Grosjean [a]

[a] Institute of Geography & Oeschger Centre for Climate Change Research, University of Bern, Hallerstrasse 12, 3012 Bern, Switzerland
[b] Geological Institute, ETH Zurich, Sonneggstrasse 5, 8092 Zurich, Switzerland
[c] Institute of Plant Sciences & Oeschger Centre for Climate Change Research, University of Bern, Altenbergrain 21, 3013 Bern, Switzerland
[d] Institute of Geological Sciences & Oeschger Centre for Climate Change Research, University of Bern, Baltzerstrasse 3, 3012 Bern, Switzerland

HIGHLIGHTS

- The XRF-Mn/Fe redox proxy is evaluated with sequential Fe and Mn fractions.
- Intensive diagenetic processes limit the use of the XRF-Mn/Fe proxy.
- Mn can be trapped in the sediments in authigenic forms under permanent anoxia.
- Catchment processes and detrital inputs highly affect Mn/Fe ratios in the sediments.

GRAPHICAL ABSTRACT

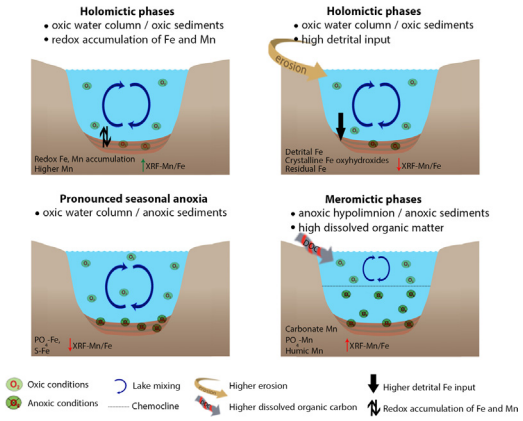

ARTICLE INFO

Article history:
Received 15 June 2020
Received in revised form 15 October 2020
Accepted 22 October 2020
Available online xxxx

Editor: Filip M.G. Tack

Keywords:
Sequential extraction
Paleolimnology
Late-Glacial/Holocene
Mn/Fe ratio
Seasonal anoxia
Meromixis

ABSTRACT

Global spread of anoxia in aquatic ecosystems has become a major issue that may potentially worsen due to global warming. The reconstruction of long-term hypolimnetic anoxia records can be challenging due to lack of valid and easily measurable proxies.

The sedimentary Mn/Fe ratio measured by X-ray fluorescence (XRF) is often used as a proxy for past lake redox conditions. Yet the interpretation of this ratio can be problematic when Fe and Mn accumulation is not solely redox driven. We used the varved sediments of Lake Moossee (Switzerland) to examine the partitioning of Fe and Mn in seven fractions by sequential extraction under various oxygen conditions over the last 15,000 years. We combined this data with XRF scans and an independent diagnostic proxy for anoxia given by a hyperspectral imaging (HSI)-inferred record of bacteriopheophytin, to validate the use of the XRF-Mn/Fe ratio as redox proxy. In the 15,000-year long record, Fe was bound to humins and amorphous, crystalline, sulfide and residual forms. Mn was mainly present in carbonate and amorphous forms. Higher erosion, prolonged anoxia, diagenesis and humic matter input affected Fe and Mn accumulation. Under holomixis the XRF-Mn/Fe ratio successfully reflected lake redox conditions. Periods with higher detrital Fe input obscured the applicability of the ratio. During phases of permanent anoxia, intensified early diagenetic processes trapped Mn in the sediments in carbonate,

* Corresponding author.
E-mail addresses: stamatina.makri@giub.unibe.ch (S. Makri), giulia.wienhues@giub.unibe.ch (G. Wienhues), moritz.bigalke@giub.unibe.ch (M. Bigalke), adrian.gilli@erdw.ethz.ch (A. Gilli), hendrik.vogel@geo.unibe.ch (H. Vogel), martin.grosjean@oeschger.unibe.ch (M. Grosjean).

https://doi.org/10.1016/j.scitotenv.2020.143418

crystalline oxide and humic forms. Our study shows that the single use of the XRF-Mn/Fe ratio is often not conclusive for inferring past lake redox conditions. The application of the XRF-Mn/Fe as a proxy for anoxia requires taking into account the individual lake characteristics and changes in lake environmental conditions, which affect the accumulation of Fe and Mn in the sediments.

1. Introduction

Oxygen is fundamental in lake systems (Wetzel, 2001), and the abundance or the lack thereof controls many chemical, biological and physical lake processes (Imboden, 1998). Oxygen regulates water column and water-sediment interface chemistry through redox processes affecting water quality, biodiversity (Nürnberg, 1995) and ecosystem services in general (United Nations, 2015). Both natural and human factors, e.g. warmer temperatures and excessive nutrient inputs can regulate the establishment of anoxic conditions in lakes (Fang and Stefan, 2009; Foley et al., 2012) mainly by enhancing thermal stratification (Woolway and Merchant, 2019) and stimulating aquatic productivity (Schindler, 2006).

The reconstruction of long-term hypolimnetic anoxia can be challenging (Friedrich et al., 2014). Jenny et al. (2013) used the onset of annual laminations as a proxy of hypoxia in lakes across the world. Other diagnostic proxies used so far, such as lipid biomarkers (Naeher et al., 2012) or pigments indicative of the presence of sulfur bacteria at the chemocline (Wirth et al., 2013), are difficult to measure. Another widely used approach is the Mn/Fe ratio inferred from scanning X-ray fluorescence (XRF) (Friedrich et al., 2014; Naeher et al., 2013), which provides semi-quantitative information about lake oxygenation from seasonal to millennial scales. The rationale of the XRF-Mn/Fe proxy is that Fe and Mn change their redox state and solubility at different rates and Eh values (redox potentials), whereby Mn is thought to be more sensitive to redox changes than Fe (Boyle, 2001; Davison, 1993). In principle, high Mn/Fe ratios may indicate increased O_2 concentrations, and low Mn/Fe ratios may indicate reducing conditions (Boyle, 2001; Mackereth, 1966; Wersin et al., 1991).

This proxy is readily measurable but is not always diagnostic and conclusive, and caveats have been reported (Friedrich et al., 2014; Naeher et al., 2013). Fe and Mn net accumulation in sediments can be controlled by several factors other than redox changes, such as clastic inputs (Dean, 2002), various biogeochemical processes in the lake water and diagenetic alterations in sediments (Davison, 1993). Lake hydrodynamics such as current or wave actions and lake bottom morphology can also affect the deposition pattern of dissolved Fe and Mn under low oxygen conditions. In this case, Fe and Mn profiles in the sediments reflect mainly their horizontal transport before deposition (geochemical focusing, Engstrom et al., 2006; Schaller and Wehrli, 1996). Engstrom et al. (2006) also stressed the difference between hypoxic or anoxic sediments overlaid by oxic or anoxic bottom waters with regard to net loss of Fe and Mn dissolved from the sediments into the hypolimnion.

Fe and Mn fractions in the sediments (Templeton et al., 2000) help us understand the geochemical processes and conditions at the time of deposition and possible subsequent diagenetic alterations in the sediment. The mobility of the two metals depends on their oxidation state, adsorption onto minerals (e.g. clays, oxides, oxy(hydr)oxides) or organic ligands, and their incorporation into mineral species. Furthermore, bacteria catalyze Fe and Mn mineral precipitation and dissolution (Brandt et al., 2017). In addition, changes in environmental conditions, such as mixing regimes and redox changes, aquatic productivity and eutrophication, lithogenic erosional input from the catchment or soil leaching, can affect the partitioning of Fe and Mn. Sequential extraction of Fe and Mn fractions has been widely applied to lake sediments to evaluate Fe and Mn sources, mobility, pathways, and potential depositional and post-depositional mechanisms related to lake internal or external processes (Adekola et al., 2010; Sobczyński and Siepak, 2001; White and Gubala, 1990).

In this study, we investigate the distribution of Fe and Mn fractions in the varved sediments of Lake Moossee in Switzerland, under various environmental conditions over the past 15,000 years. We address the following questions: 1) How did changing catchment processes and lake biogeochemical cycles influence net burial rates and partitioning of Fe and Mn in postglacial times? 2) What are the conditions under which XRF-Mn/Fe ratios provide reliable information about past lake water oxygenation? We use a sequential extraction method modified from Hall et al. (1996) to measure seven Fe and Mn fractions, combined with scanning XRF elemental data, TOC, TIC and an existing record of anoxia inferred from sedimentary pigments (Makri et al., 2020). Lake Moossee was selected because its postglacial 15,000-year long history covers a wide range of possible lake states from fully clastic to biogenic depositional environments, well oxygenated to meromictic conditions, and oligotrophic to hypertrophic states in a landscape that developed from tundra to closed forest and, later, to an open landscape under growing anthropogenic pressure. All of these processes are thought to influence sedimentary Fe and Mn fractions in different ways.

2. Materials and methods

2.1. Study site

Lake Moossee (47°1′17.0″N, 7°29′1.7″E) is a small exorheic lake of glacial origin on the western Swiss Plateau, at 521 m.a.s.l. (Fig. 1A). Its maximum depth is 22 m, and the surface area is 0.31 km^2 (length: 1.1 km, max. width: 300 m) (Fig. 1B) (Guthruf et al., 1999). Lake Moossee is currently eutrophic and typically dimictic, with a short turnover in late autumn and a more intensive spring turnover (Guthruf et al., 1999, 2015). The epilimnion is about seven times larger than the hypolimnion, which favors oxygen depletion in the bottom waters during summer stratification (Guthruf et al., 1999). The catchment bedrock is composed of Tertiary molasse calcareous sandstone overlain by glacial till, fluvioglacial sediments and loess loam (Schmid et al., 2004). Histosols, Gleysols and Luvisols developed in the catchment ("Geoportal des Kantons Bern", 2019).

The catchment (20.8 km^2) is, today, mostly used for intensive agriculture (Guthruf et al., 1999). Mixed beech forests cover the hills, while alder and ash cover the lake shore (Rey et al., 2019a). Annual mean temperature is 8.8 °C, and annual mean precipitation amounts to 1057 mm (Bern/Zollikofen station, MeteoSwiss, 2019). Significant human activity around the lake took place since the Neolithic and Bronze Age (Harb, 2017).

2.2. Composite sediment profile, chronology and lithology

In this study, we used the ~10 m long composite sediment core introduced by Makri et al. (2020). In 2014, Rey et al. (2020, 2019b) retrieved five parallel sediment cores in the southern deeper part of the lake (Fig. 1B), and established a high-precision radiocarbon chronology combined with varve counting and wiggle-matching approaches (Rey et al., 2019b). For the top 7 m of the composite core used for this study, the age–depth model (Fig. 1C; Makri et al., 2020) is based on linear interpolation of 100 tie points with the dated cores from Rey et al. (2020). From 7 m to the bottom, the cores and chronology are identical

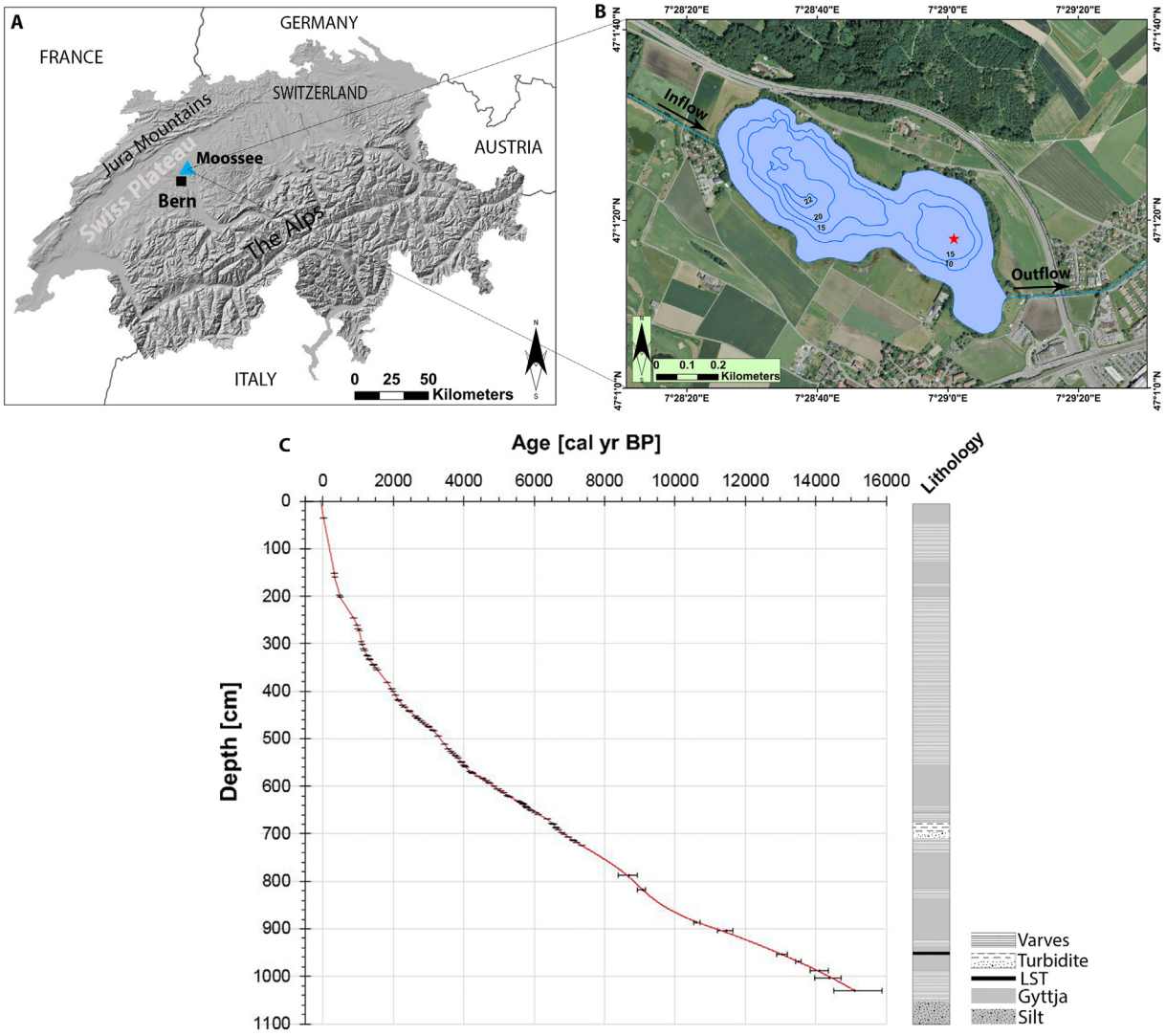

Fig. 1. A) Location of Lake Moossee. B) Lake bathymetry indicating the coring position with a red star (modified from Makri et al., 2020). C) Age-depth model and lithology from Makri et al. (2020). LST is the Laacher See tephra. (For interpretation of the references to color in this figure legend, the reader is referred to the web version of this article.)

with the ones used in Rey et al. (2020). A detailed description of the chronology and a full list of the 60 radiocarbon dates used are found in Rey et al. (2020, 2019b).

The sediments are almost entirely laminated interrupted by a few parts with homogenous sedimentation of silt (at the bottom) or gyttja with diffuse laminations upcore (Fig. 1C; Makri et al., 2020). As shown in Fig. 1C, around 13,034 cal BP, a distinctive blue-greyish (GLEY2 5/1; Munsell Color (Firm), 2010) layer is attributed to the Laacher See Tephra. Around 9700 cal BP, a large turbidite (20 cm) interrupted regular sediment deposition.

2.3. Geochemical analysis

Scanning X-ray fluorescence (XRF) was performed at continuous 1 mm steps with the Avaatech core scanner at ETH Zurich. We measured an area of 1 mm by 12 mm for 20 s at 10 kV (1500 μA) and at 30 kV (2000 μA), and the results are given as counts (peak area). In total, 43 discrete sediment subsamples (1-cm thick slices) were taken along the core with higher sampling density in sections with large gradients in the composition of XRF and anoxia data (Makri et al., 2020), and in the past 500 years. The outer oxidized layers of the slices were removed and the subsamples were freeze-dried and homogenized. Additional XRF measurements were performed on the same 43 discrete subsamples taken for the sequential Fe and Mn extraction. These subsamples were scanned in sample boxes at continuous 2 mm steps using the ITRAX μXRF core scanner at the University of Bern, equipped with a Mo-tube (exposure time 20 s, 30 kV and 50 mA). These data were used for statistical analysis (see Supplementary material Fig. S1). Titanium serves as a proxy for erosional input (Koinig et al., 2003). Calcium is associated to calcite abundance (Koinig et al., 2003; Makri et al., 2020). Both S and P bind to Fe and Mn, and form compounds of different stability affecting their distribution and mobility in the sediments. These elements are used as independent proxies of specific conditions for the formation of different Fe and Mn fractions.

Total organic carbon (TOC) and inorganic carbon (TIC) were determined by loss on ignition (LOI550°C, LOI950°C) following Heiri et al. (2001). Total nitrogen was measured with a CNS-Analyzer (Elementar vario EL cube). The TOC/TN ratio was used to make inferences about organic matter sources (Meyers, 2003).

Seven fractions (F1–F7, Fig. 2) of Fe and Mn were determined following a modified sequential extraction procedure by Hall et al. (1996). We added three extraction steps: PO_4-Fe and Mn (F1; Gu et al., 2016), humic Fe and Mn (F3, Hall and Pelchat, 1997), and residual Fe and Mn minerals (F7). The pyrophosphate leach (F3) was

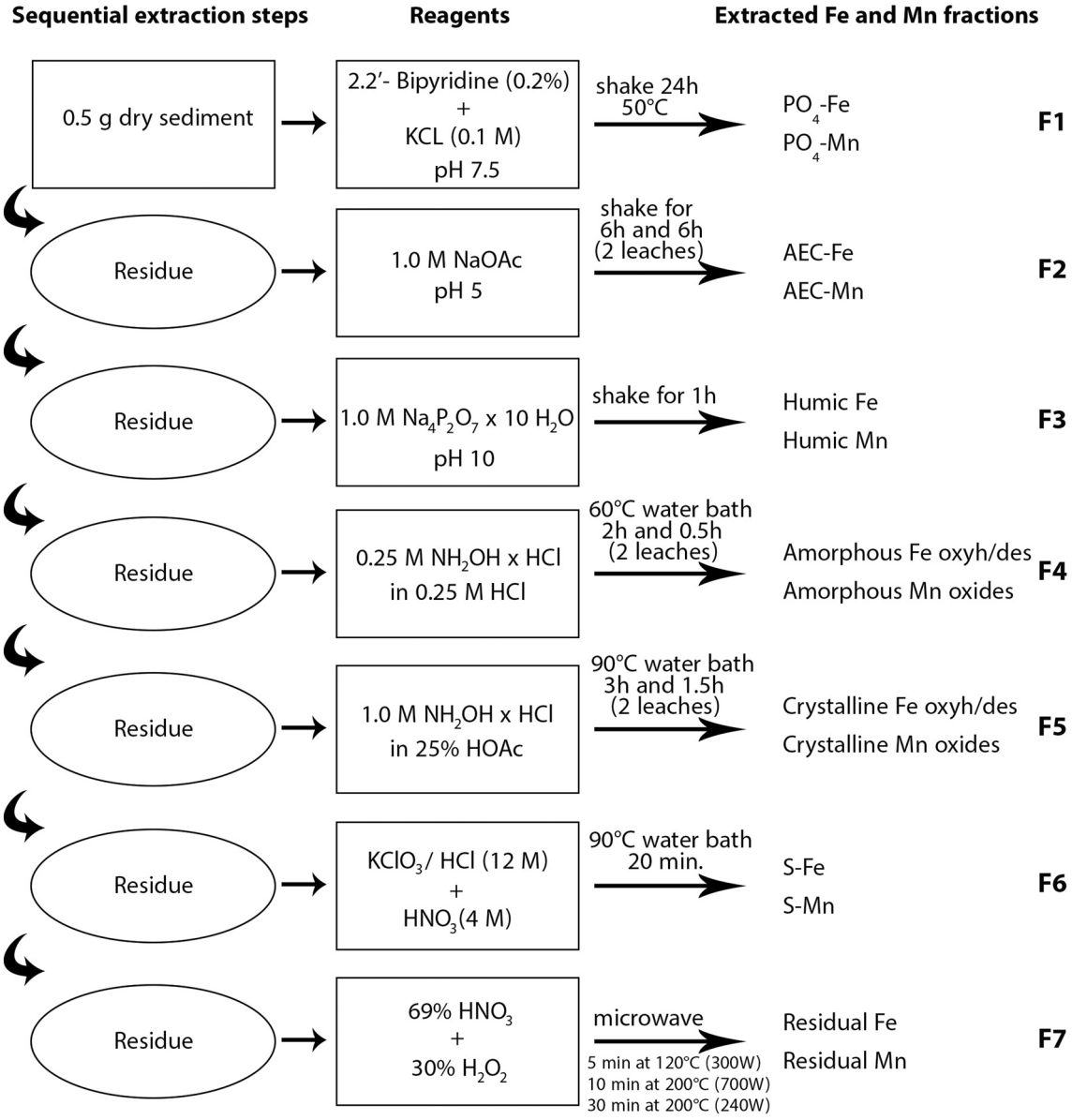

Fig. 2. Scheme of the sequential extraction of the seven Fe and Mn fractions modified from Hall et al. (1996), Hall and Pelchat (1997), and Gu et al. (2016). AEC: adsorbed/exchangeable/carbonate phase. NaOAc: sodium acetate.

applied to avoid overestimation of the Fe oxy(hydr)oxide and Mn oxide fraction (F4) in organic-rich sediments due to labile organic components (Hall et al., 1996). In order to assure adequate dissolution of the Fe oxy(hydr)oxide and Mn oxide fraction (F4), minimize an early dissolution of the sulfides fraction (F6) and a redistribution of Fe and Mn concentrations among these fractions, we applied the best fitting extraction configuration (Fig. 2) based on the extensive validation steps by Hall et al. (1996).

For the sequential extraction, we used 0.5 g of the 43 freeze-dried homogenized sediments samples. All reagents were Roth (Carl Roth GmbH + Co. KG, Karlsruhe Germany) and Sigma-Aldrich (Merck KGaA, Darmstadt, Germany) American Chemical Society (ACS) reagent grade. Ultrapure water of 18.2 Mohm-cm at 25 °C (Milli-Q) was used throughout the steps. The comparison between the sums of the seven fractions with the total digestion revealed differences of 8% for Fe and 1% for Mn (Figs. S2, S3a and b in Supplementary material). The accuracy of the analysis was checked by digesting the certified reference material San Joaquin Soil (SRM2709a, NIST, Boulder, CO). The results yielded, on average, ca. 95% and 92% of the certified reference values for Mn and Fe, respectively (Table S1 Supplementary material). Element concentrations were measured by inductively coupled plasma mass spectrometry (ICP-MS; 7700x, Agilent, Palo Alto, CA) with a collision cell in helium mode, using ^{103}Rh and ^{115}In as internal standards. Before injection, the leachates were diluted using factors ranging from 100 to 2000. Triplicate sample measurements were made every 10th sample for quality control and the general reproducibility of the analysis yielded very good results between 3 and 10%. The average relative standard deviation of these measurements for each fraction is given in Supplementary material Table S2.

The extraction steps enabled the identification of seven Fe and Mn fractions (F1–F7, Fig. 2):

F1: PO_4-Fe and PO_4-Mn, such as vivianite ($Fe_3^{2+}(PO_4^{3-})*8H_2O$) or phosphoferrite ($(Fe^{2+}, Mn^{2+})_3(PO_4)_2*3H_2O$), are authigenic minerals (Håkanson and Jansson, 1983) formed under reducing conditions in sulfide-depleted pore waters rich in Fe^{2+} and PO_4^{3-} (Berner,

1981; Nriagu and Dell, 1974). The presence of these minerals in the sediments can, therefore, reflect anoxic non-sulfidic bottom waters (Nriagu, 1972). In the sediments of Lake Moossee, vivianite concretions were confirmed after identification in smear slides.

F2: AEC-Fe, AEC-Mn (adsorbed/exchangeable/carbonate) phase, refers mainly to Fe and Mn bound to carbonates, such as siderite ($FeCO_3$) and rhodochrosite ($MnCO_3$). They are formed in the sediments or at the sediment-water interface under reducing conditions (Håkanson and Jansson, 1983), and sufficiently high concentrations of Fe^{2+} or Mn^{2+} and bicarbonate (Stevens et al., 2000; Wetzel, 2001). Mn carbonates tend to be more pH dependent with better solubility at very low pH levels (Stevens et al., 2000; Tribovillard et al., 2006).

F3: Humic Fe and humic Mn refer to strong complexes of Fe and Mn with organic compounds (Hall and Pelchat, 1997). They are mainly endogenously formed under alkaline and oxic conditions, and high content of humic and fulvic acids (Nurnberg and Dillon, 1993; Shaw, 1994). Organic acids are adsorbed onto the freshly formed Fe oxy(hydr)oxides and Mn oxides and form complexes that gradually precipitate to the sediments (Wetzel, 2001).

F4: Amorphous Fe oxy(hydr)oxides and amorphous Mn oxides occur under oxic conditions and are much more labile than crystalline Fe oxy(hydr)oxides and Mn oxides (Martynova, 2010). Under anoxic conditions, amorphous phases are reductively dissolved releasing Fe^{2+} and Mn^{2+}, which may re-oxidate and re-precipitate as authigenic Fe oxy(hydr)oxides and Mn oxides in oxic waters (Davison, 1993; van der Zee et al., 2003).

F5: Crystalline Fe oxy(hydr)oxides and crystalline Mn oxides such as goethite (FeOOH), hematite (Fe_2O_3) or birnessite (Na,Ca $Mn_7O_{14}{*}3H_2O$) are thermodynamically stable endmembers (Cornell and Schwertmann, 2003; Wetzel, 2001). They constitute a continuum from amorphous to crystalline forms (van der Zee et al., 2003). Their source is mainly allogenic (Håkanson and Jansson, 1983). Their formation, mainly that of manganese oxides, requires bacteria to catalyze the oxidation of manganous ions in sediments and soils (Tipping et al., 1985).

F6: S-Fe and S-Mn refer to iron and manganese bound to sulfides. These are formed in anoxic sediments after the reduction of sulfate (SO_4^{2-}) to sulfide (S^{2-}) which is often related to microbial activity (Håkanson and Jansson, 1983). Fe sulfides are found as acid volatile sulfides (AVS) or pyrite. The presence of mainly ferrous iron in the sediments under anoxic conditions leads to the initial precipitation of pyrrhotite (FeS) that transforms gradually to pyrite (FeS_2) (Hamilton-Taylor and Davison, 1995). AVS are less stable than pyrite and vulnerable to early dissolution in the sequential extraction process (Peltier et al., 2005) or during sediment preparation (Rapin et al., 1986). Thus, F6 should consist mainly of authigenic pyrite, which is insoluble under ambient conditions and stable to redox and pH condition changes.

F7: Residual Fe and residual Mn refer to iron and manganese bound to other more stable minerals and can be considered as exclusively allogenic (Håkanson and Jansson, 1983). This fraction does not contain Fe and Mn included in the structure of stable silicates, as no HF was used for the digestion, but may consist of Fe and Mn in unstable silicates, oxides, oxy(hydr)oxides. While the exact composition of this fraction is not known, it is clear that this fraction is composed of very inert minerals. The structure of this fraction does not change during deposition, which makes it useful for the evaluation of catchment erosion.

Not all fractions are affected by redox conditions in the lake water. Among the seven fractions, we consider fraction F4 (F4-$Fe_{oxy(hydr)oxides}$, F4-Mn_{oxides}, and their ratio) as the most adequate indicator of bottom water oxygenation. However, Fe and Mn redistribution in this phase due to an early dissolution of sulfides found in a very labile form in anoxic sediments, particularly sphalerite (ZnS) (Hall et al., 1996; Larner et al., 2008), can potentially limit the use of this fraction (Peltier et al., 2005). For past hypolimnetic anoxia and mixing regime changes, we use the independent proxy given by the HSI-inferred record of bacteriopheophytin (Bphe) from Makri et al. (2020), and we include F4 in the multivariate statistical analysis for further inference.

2.4. Statistics

Statistical analysis was performed in R (R Core Team, 2015). Constrained hierarchical clustering (euclidean distance and coniss linkage method in R) was applied on the seven Fe and Mn fractions, selected XRF data (Ti, Ca, P, S), TOC, TIC and TOC/TN to define the units. A principal component analysis (PCA) was performed on a synthesis dataset, which consisted of the dataset mentioned above plus TChl (chlorophyll *a*, *b* and derivatives; proxy for aquatic production) and Bphe (proxy for anoxia) from Makri et al. (2020). Constrained hierarchical clustering was also performed on the synthesis dataset. The broken stick model was used to determine the significant groups in the cluster analysis and to assess the likely statistical significance of the axes in the PCA. Data were log transformed to stabilize their variance and then standardized prior to statistical analysis.

3. Results

3.1. Fe and Mn fractions and other geochemical proxies

Fig. 3A shows the relative values of the Fe and Mn fractions in the sediments of Lake Moossee for the last 15,000 years cal BP. Overall, Fe is mainly present in the amorphous oxy(hydr)oxide (F4, av. ~42%) and crystalline oxy(hydr)oxide (F5, av. ~32%) forms, followed by humic (F3, av. ~10%), residual (F7, av. ~6%), and S-Fe (F6, av. ~5%) (Fig. 3A). AEC-Fe (F2) is very low compared to the values of the other fractions. Iron fractions show strong variability across the four units covering the last 15,000 years. In unit I, corresponding to the late Oldest Dryas, crystalline oxy(hydr)oxides (F5) and residual Fe (F7) dominate (sum av. ~62%), amorphous Fe oxy(hydr)oxides (F4) and S-Fe (F7) are present in lower proportions. In unit II, corresponding to Bølling/Allerød and Younger Dryas, amorphous Fe oxy(hydr)oxide (F4) is most abundant (av. ~73%), followed by crystalline oxy(hydr)oxide forms (F5, av. ~18%). Residual Fe oxides (F7) and S-Fe (F6) disappear, and traces of humic forms (F3) emerge. In unit III, corresponding to the Holocene, amorphous Fe oxy(hydr)oxide (F4) still dominates until 5500 cal BP (av. ~48%), followed by crystalline oxy(hydr)oxide forms (F5, av. ~30%); humic forms (F3) show a marked relative increase after 5500 cal BP (av. ~12%). Residual Fe (F7) and S-Fe (F6) are absent in the first part of unit III and only appear in traces after 5500 cal BP. In unit IV, corresponding to the last 500 years, crystalline oxy(hydr)oxide (F5) and amorphous oxy(hydr)oxide (F4) forms prevail (sum av. ~64%). Residual Fe (F7) and S-Fe (F7) increase their relative abundance, and humic forms (F3) decrease.

The overall patterns for Mn relative values differ substantially from those of Fe (Fig. 3A). Throughout the record, Mn is almost exclusively found in the amorphous oxide (F4, av. ~54%) and AEC (F2, av. ~37%) forms. Noticeable amounts of residual Mn (F7) and crystalline Mn oxides (F5) are only found in unit I (sum. av. <18%). In unit III, AEC-Mn (F2, av. ~47%) is higher than amorphous Mn oxides (F4, av. ~44%).

Fig. 3B shows the concentrations of the seven Fe and Mn fractions across the four units. PO_4-Fe, PO_4-Mn (F1, Fig. 3B) show minimum values in unit I. In unit II, both increase significantly with PO_4-Mn reaching maximum values around 14,300 cal BP. TOC increases in this unit, whereas TIC and Ca remain low (Fig. 3C). In unit III, from ca. 5500 to 500 cal BP, PO_4-Fe shows distinct peaks reaching maximum

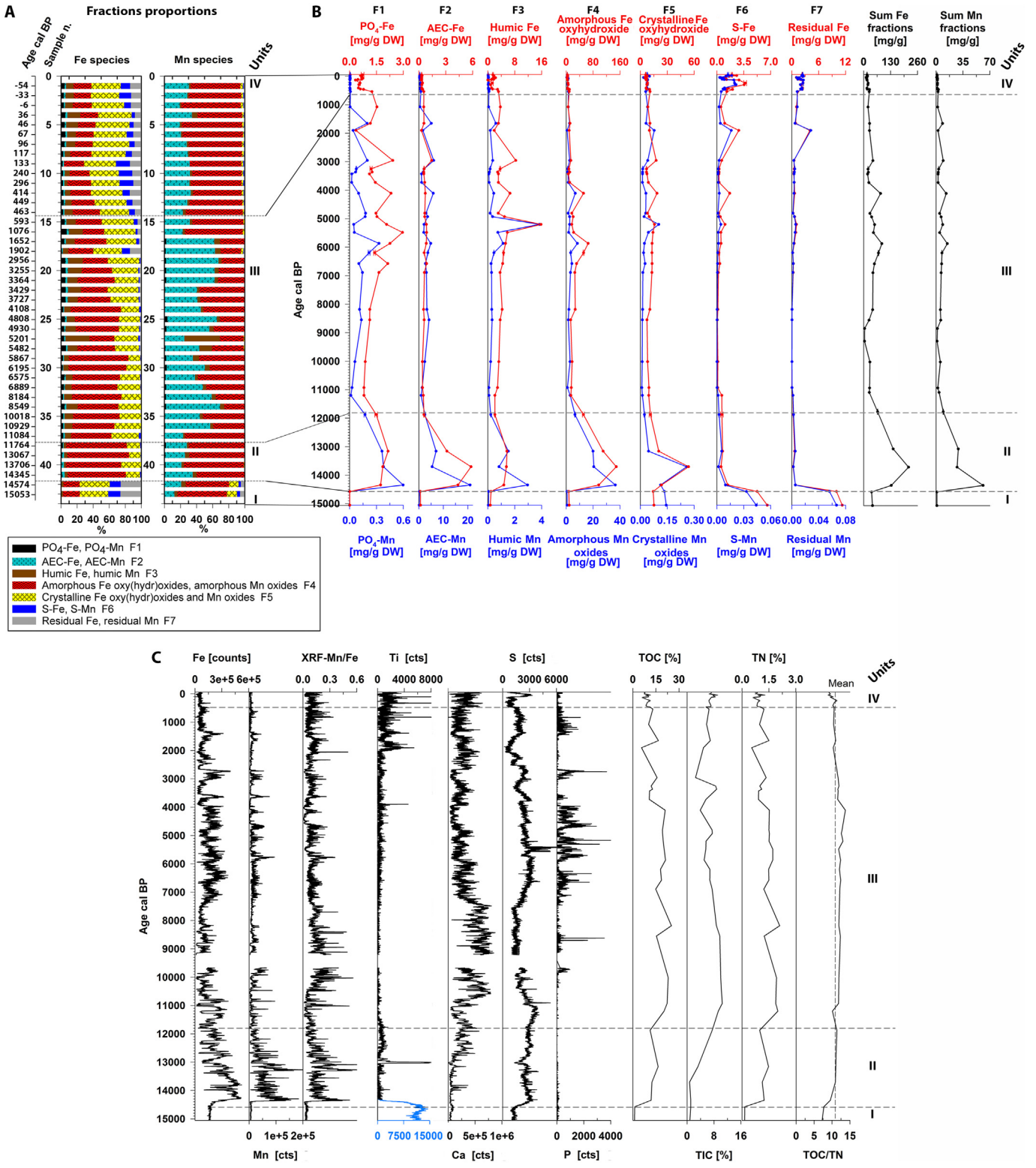

Fig. 3. A) Relative values of Fe and Mn fractions (F1–F7) in the sediments of Lake Moossee. B) Concentrations of Fe and Mn in the seven fractions. C) XRF element counts, TOC and TIC values. In the Ti profile (Makri et al., 2020), the blue color refers to the scale at the bottom. The units are defined by constrained hierarchical clustering. (For interpretation of the references to color in this figure legend, the reader is referred to the web version of this article.)

values, which coincide with higher P counts (Fig. 3C). PO_4-Mn shows often opposite trends. In unit IV, both fractions show low concentrations. Vivianite concretions were microscopically identified around 2730 cal BP, 3785 cal BP, and between 5547 and 5677 cal BP.

AEC-Fe and AEC-Mn (F2, Fig. 3B) show minimum values in unit I. In unit II, both increase; AEC-Mn reaches maximum values around 14,300 cal BP, whereas AEC-Fe reaches maximum values around 13,600 cal BP. In unit III, between ca. 5500 to 1000 cal BP, AEC-Mn

shows distinct relative maxima. In unit IV, both AEC-Fe and AEC-Mn have very low values.

Humic Fe and humic Mn (F3, Fig. 3B) exhibit minimum values in unit I. In unit II, both increase, and humic Mn reaches maximum values around 14,300 cal BP. In unit III, between 5500 and 500 cal BP, humic Fe shows distinctive peaks and overall highest values. TOC/TN ratio is also higher during this time (Fig. 3C). Humic Mn remains generally low, with a peak around 5500 cal BP. In unit IV, both humic Fe and Mn have low concentrations.

Amorphous Fe oxy(hydr)oxides and amorphous Mn oxides (F4, Fig. 3B) exhibit overall similar patterns. Their concentrations are minimal in unit I. In unit II, both increase sharply and reach maximum values, around 14,300 cal BP for amorphous Mn oxides and around 13,600 cal BP for amorphous Fe oxy(hydr)oxides. In unit III and IV, both have lower concentrations, showing two local maxima at around 6000 and 4000 cal BP.

Crystalline Fe oxy(hydr)oxides and crystalline Mn oxides (F5, Fig. 3B) show the same pattern. Both have moderate concentrations in unit I. In unit II, they increase to peaks around 13,600 cal BP and then decrease to low levels. In unit III, between ca. 5500 and 1500 cal BP, concentrations of crystalline Fe oxy(hydr)oxides and Mn oxides increase slightly. Thereafter, and in unit III, they decrease and remain constantly low.

The S-Fe, S-Mn (F6, Fig. 3B) exhibit maximum concentrations in unit I. Titanium also has maximum values in this part, whereas S is present but with low values (Fig. 3C). In unit II, both S-Fe and S-Mn decrease significantly. In unit III, S-Fe is present with very low concentrations and decreases to minimum values around 11,000 cal BP. Sulfur counts increase in unit II and decrease around 11,000 cal BP. Between ca. 6000 and 3000 cal BP, S-Fe shows some variations with higher values, whereas S-Mn has very low values. Around 2000 cal BP both S-Fe and Mn show a relative maximum that coincides with higher Ti counts. In unit IV, concentrations of S-Fe and Mn increase, showing a distinctive local maximum around 250 cal BP.

Residual Fe and residual Mn (F7, Fig. 3B) show maximal values in unit I. In unit II and most of unit III, both residual Fe and Mn have very low to minimal values. Around 2000 cal BP, both increase showing a distinctive local maximum and then decrease with low values until present (unit IV).

XRF Fe and Mn values (Fig. 3C) show the same pattern as the sum of the seven fractions after sequential extraction (Fig. 3B), as well as the concentrations after total digestion (Fig. S2 Supplementary material). The XRF-Mn/Fe ratio is lowest in unit I and has generally higher values in unit II and in the first half of unit III until 7000 cal BP. Between 7000 and ca. 1500 cal BP, it remains relatively low with increased variability. After 1500 cal BP, the XRF-Mn/Fe ratio slightly increases until ca. 250 cal BP when it decreases again.

3.2. Relationships of Fe and Mn fractions with lake and catchment processes

To analyze the relationships of Fe and Mn fractions with changes in lake biogeochemistry and catchment processes, we performed a PCA on our data set (Fig. 3) in combination with existing data of aquatic production (TChl) and anoxia/meromixis (Bphe) from Makri et al. (2020).

Fig. 4A shows the PCA biplot of the first two significant components, PC1 (46.32%) and PC2 (24.88%), as indicated by the broken stick model. Together, these explain ca. 71% of the total variance. PO_4-Fe (F1), humic Fe (F3) and AEC-Mn (F2) and the sum of sequentially extracted Mn (SE-Mn_{sum}) are grouped and correlate positively with PC1. These fractions are related to Bphe, S, TOC, and TOC/TN, which indicate anoxic and reducing bottom water and sediments, and presence of increased dissolved organic matter. PO_4-Mn (F1), humic Mn (F3), amorphous Fe oxy(hydr)oxides and Mn oxides (F4), and AEC-Fe (F2) are grouped and correlate positively with PC1. These fractions are related more to P and less to Bphe than the previous group; this indicates better bottom water oxygenation, reducing sediments, and enhanced diagenetic processes. The correlation of these groups with the XRF-Mn and the SE-Mn_{sum} indicates that diagenetic processes play an important role in Mn accumulation in the sediments. The F4-$Mn_{oxides}/Fe_{oxy(hydr)oxides}$ ratio correlates negatively with PC1 and indicates oxic conditions. Interestingly, the XRF-Mn/Fe and F4-Mn/Fe ratios anticorrelate, and the XRF-Mn/Fe ratio is associated with variables indicating anoxic conditions in the hypolimnion. PC1 reflects a gradient from oxic to anoxic conditions associated with lake mixing and bottom water oxygenation (Fig. 4B).

S-Fe and S-Mn (F6) and residual Fe and Mn (F7) form another group and correlate negatively with PC2. These fractions are strongly related to Ti, which signals their dependence on higher detrital input. However, these fractions seem to be independent of both carbonate deposition (TIC, Ca) and lake production (TChl). Crystalline Mn oxide (F5) correlates negatively with PC2, is negatively related to carbonates (TIC, Ca) and lake production (TChl), and independent of both lake mixing and water column oxygenation (Bphe). Crystalline Fe oxy(hydr)oxide (F5) is also independent of lake mixing and oxygen changes (Bphe) and seems to be affected by detrital input and to some extend diagenetic processes. The XRF-Fe and SE-Fe_{sum} relate closely to F5, suggesting a stronger dependence of Fe accumulation to detrital than redox conditions. PC2 reflects a gradient from high to low production, carbonates content, and erosional input (Fig. 4B).

4. Discussion

The Mn/Fe ratio measured by XRF has been used extensively as a proxy for bottom water oxygenation and redox conditions changes (Koinig et al., 2003; Loizeau et al., 2001; Naeher et al., 2013; Żarczyński et al., 2019). Most of these studies used a multiproxy approach for the interpretation of the Mn/Fe ratio as a redox proxy. Comparing Fe and Mn fractions with an independent proxy for anoxia, the HSI-inferred Bphe record (Makri et al., 2020), enables the validity of XRF-inferred Mn/Fe ratio as a proxy for anoxia to be examined (Fig. 5). Nonetheless, certain deficiencies should not be overlooked.

The sequential extraction scheme likely involves some uncertainties. The degree of these uncertainties is normally depending on sediment matrix, i.e. organic matter content, redox conditions (Hall et al., 1996), or affected by sample preparation (Rapin et al., 1986). In our case, we took into consideration the high organic matter content of our sediment cores and added the pyrophosphate leach (F3) before the Fe oxy(hydr) oxides and Mn oxides phase (F4). With this additional extraction step, we avoided an overestimation of F4 due to the release of labile organic compounds. Another reported deficiency is an early dissolution of Fe and Mn sulfides (F6) during the hydroxylamine hydrochloride leach used for the extraction of fraction F4. At the same time, an adequate dissolution of the crystalline oxide fraction (F5) needs to be ensured. Based on the extensive testing from Hall et al. (1996) and Hall and Pelchat (1997) we implemented the approach that performed best (Fig. 2). Nonetheless, an early dissolution of acid volatile sulfide compounds cannot be excluded. Studies have shown that this mainly concerns ZnS forms, yet a dissolution of labile FeS forms can be also expected at a lower extent (Hall et al., 1996; Larner et al., 2008; Peltier et al., 2005). The HSI-Bphe record can be also subjected to certain limitations. The presence of anoxygenic phototrophic bacteria proves the establishment of anoxic conditions (Imhoff, 2014; Tonolla et al., 2003), yet their absence may not necessarily imply the presence of oxic conditions since these bacteria are also dependent on light and nutrient availability.

As the PCA shows (Fig. 4), surface processes, diagenetic transformation, and humic matter interactions influence the net burial rates of Fe and Mn and can obscure the interpretation of the XRF-Mn/Fe ratio as a redox proxy (Fig. 5). Residual Fe and Mn, and crystalline Fe oxy (hydr)oxides and Mn oxides (fractions F7 and F5) are primarily sourced from the catchment soils. S-Fe(Mn), PO_4-Fe(Mn) and AEC-Fe(Mn) (fractions F6, F1 and F2) suggest anoxia in the sediment and early diagenetic processes, whereas humic Fe and Mn (fraction F3) is related to

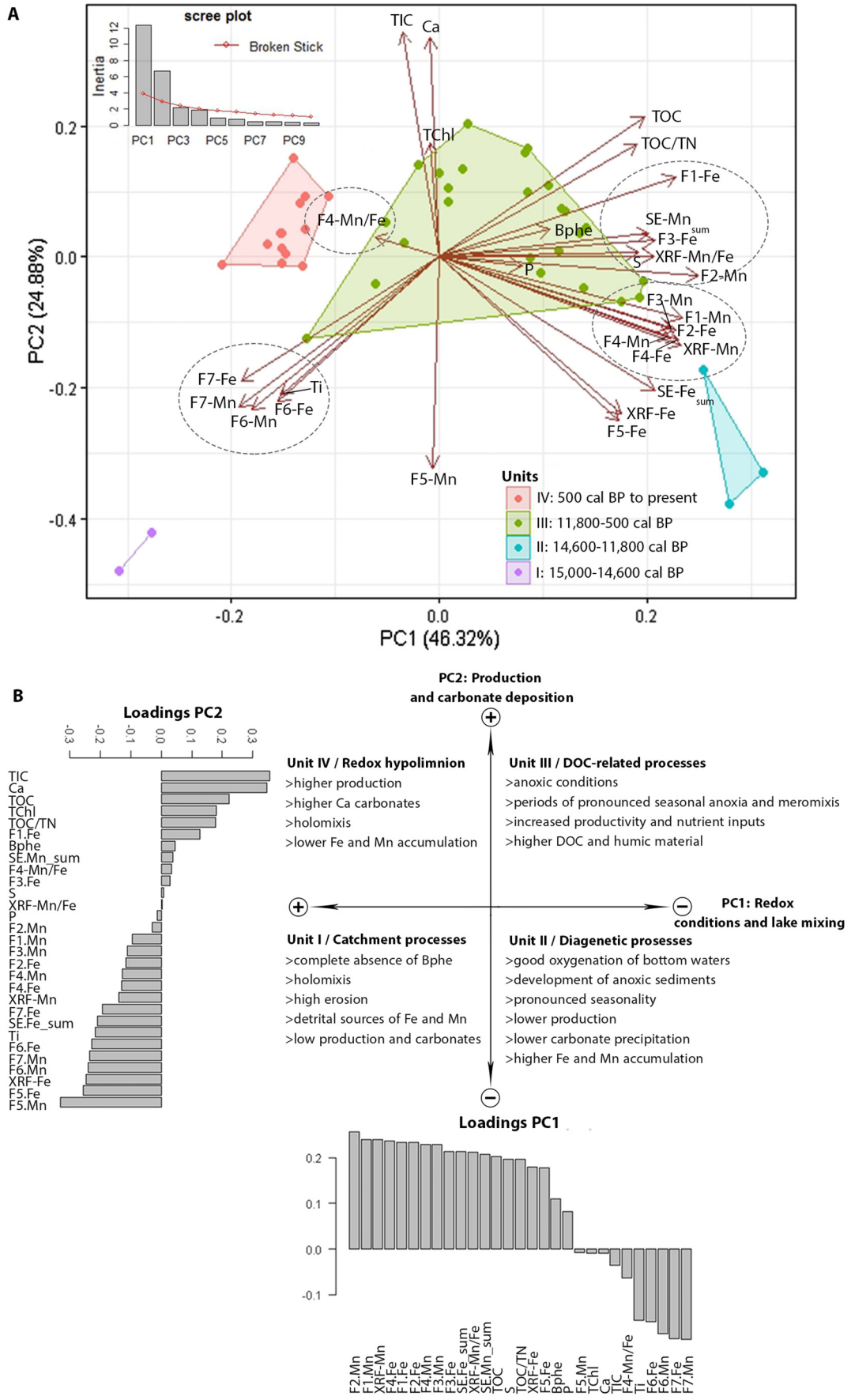

Fig. 4. A) PCA biplot showing the first two significant components PC1 and PC2, as indicated by the broken stick model (upper left). The samples are grouped by constrained clustering and are shown in different colors. B) Illustration of the inferences made by PC analysis along with loadings for PC1 and PC2.

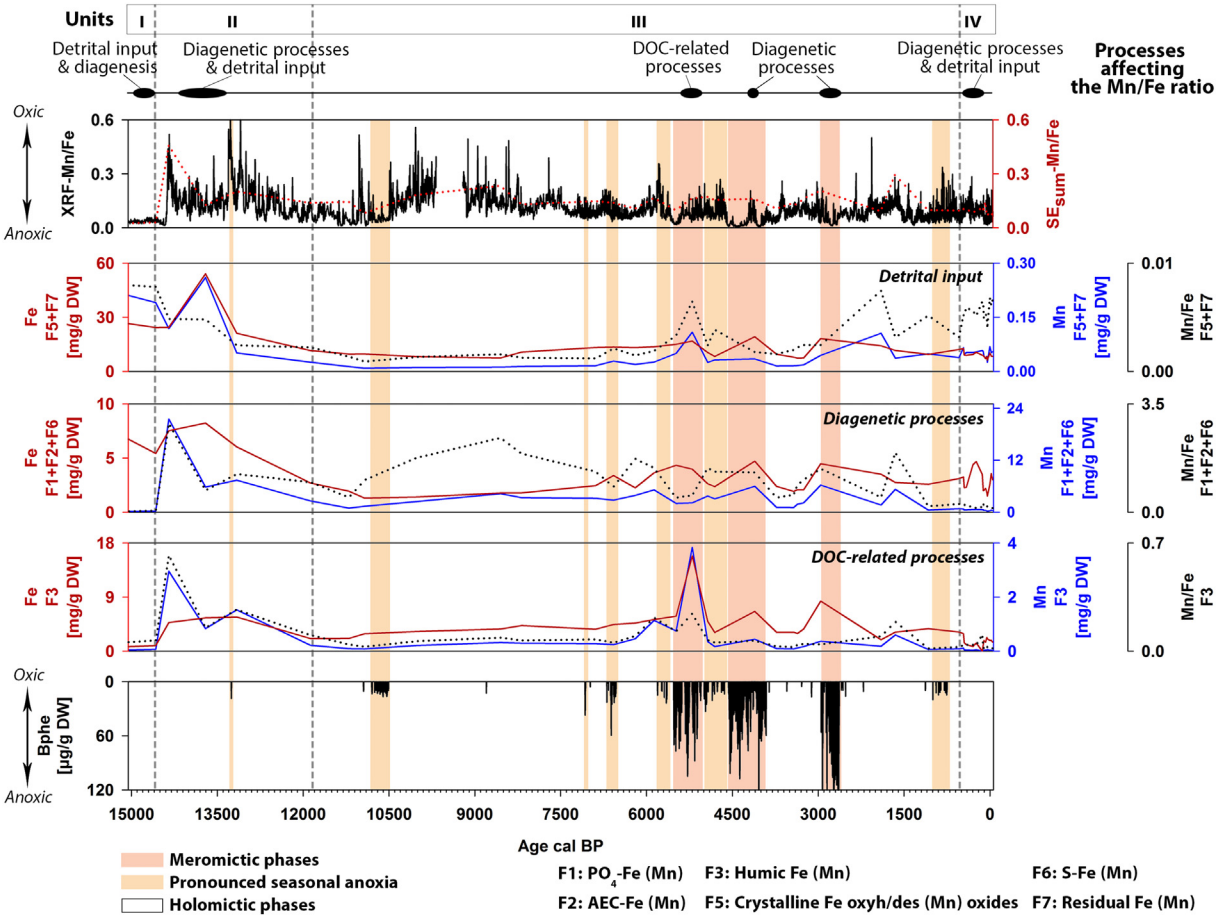

Fig. 5. Comparison of the XRF-Mn/Fe ratio with the independent proxy for anoxia given by the HSI-inferred Bphe record (Makri et al., 2020). The fractions are grouped according to the processes that can affect the accumulation of Fe and Mn in the sediments and alter the redox signal. Top: indication of the timing that these processes obscure the use of the XRF-Mn/Fe ratio as a redox proxy. Bottom: Mixing regimes according to the HSI-inferred pigment record (Makri et al., 2020). The dotted lines show the Mn/Fe ratios for every process with a detached scale on the right. For the XRF-Mn/Fe ratio (top panel), the red dotted line indicates the Mn/Fe ratio of the sum of Fe and Mn after sequential extraction (SE_{sum}-Mn/Fe). The units are defined by constrained clustering and are shown by vertical dashed lines. (For interpretation of the references to color in this figure legend, the reader is referred to the web version of this article.)

dissolved organic carbon (DOC) in the lake and leaching from soils and wetlands.

Residual Fe and Mn (F7) and crystalline Fe oxy(hydr)oxides and Mn oxides (F5) are mainly associated with detrital input in the lake and thus formation under periods of higher erosion (Figs. 4 and 5). These processes are stronger in unit I (late Oldest Dryas), in unit II between ca. 14,300 and 13,200 cal BP (Bølling/Allerød), and in unit III around 1900 cal BP (Roman Times). Fe and Mn seem to respond similarly to catchment processes, though Fe accumulation is considerably higher. Crystalline Fe oxy(hydr)oxides and Mn oxides are generally stable under all prevailing redox conditions (Hongve, 1997). These processes affect the accumulation of Fe and Mn in the sediments, thus interfering with the XRF-Mn/Fe ratio as a redox signal. This interference occurs during the late Oldest Dryas (unit I), when the XRF-Mn/Fe ratio is lowest and, Ti is highest, while the absence of Bphe indicates good oxygenation of the water column. During this time, residual Fe and Mn, and Ti are at their maximum suggesting a predominance of detrital mineral deposition (Fig. 3B and C). In the Bølling/Allerød (unit II), the XRF-Mn/Fe ratio decreases after a peak, while the absence of Bphe indicate oxic conditions in the bottom waters (Fig. 3B and 5). The Mn/Fe ratio is lower mainly due to higher allogenic input of crystalline Fe oxy(hydr)oxides in the sediments. Periods of higher detrital input effects can be easily distinguished and corrected by normalization with Ti (Kylander et al., 2011; Vegas-Vilarrúbia et al., 2018), as can be clearly seen in the Fe/Ti and Mn/Ti ratios (Fig. S4, Supplementary material).

PO_4-Fe and PO_4-Mn (F1), and AEC-Fe and AEC-Mn (F2) are mainly linked to diagenetic processes in the sediments, which suggest accumulation of these fractions in anoxic sediments (Figs. 4 and 5). These conditions are prominent in unit II between 14,300 and 13,200 cal BP (Bølling/Allerød), and in unit III at instances between ca. 7000 to 2000 cal BP. PO_4-Fe and PO_4-Mn (F1) can be formed in anoxic non-sulfidic sediments with high phosphate and Fe^{2+} content through active microbial mineralization and methanogenesis (Gächter and Müller, 2003; Lazzaretti et al., 1992; Rothe et al., 2014). Yet the distributions of Fe and Mn in these fractions show distinct differences during periods of intensive diagenetic processes. PO_4-Fe is associated with TOC and limited mixing (Bphe) and hence persistent anoxic conditions in the sediments and bottom waters (Fig. 4). PO_4-Mn is associated with P, amorphous Mn oxides and Fe oxy(hydr)oxides, and total Mn, suggesting accumulation under reducing conditions in the sediments below a probable oxygenated water body. Fe has been proven to strongly influence P cycling via formation of insoluble phosphate minerals such as vivianite (Hongve, 1997; Rothe et al., 2014; Tribovillard et al., 2006; Vuillemin et al., 2020). Formation of manganese phosphates also takes place (Hongve, 1997), yet their solubility is higher than that of Fe phosphates (Bortleson and Lee, 1974). AEC-Mn (F2) is also formed in anoxic sediments when there is sufficient reduced Mn and alkalinity.

The stability of the pH-Eh balance is very important in this case and can be affected by a balanced bicarbonate content. The bicarbonate content can be regulated by other common reactions initiated in anoxic sediments such as ammonification and sulfate reduction (Dhir, 2018; Stevens et al., 2000). Iron is more chalcophile compared to Mn and is therefore more likely to form sulfides instead of carbonates. In the Bølling/Allerød (unit II), the XRF-Mn/Fe ratio decreases in a period of oxic conditions in the hypolimnion, yet development of anoxic sediments (Fig. 5). Increased PO_4-Fe formation contributes to higher Fe accumulation in the sediments, altering the Mn/Fe ratio. During the meromictic phase from ca. 2950 to 2650 cal BP in unit III, the XRF-Mn/Fe ratio shows an increase in the first half of this period, whereas Bphe indicates persisting anoxia. The same pattern is also observed around 4100 cal BP, during a meromictic phase (from 4550 to 3900 cal BP). In the latter case, a simultaneous increase in amorphous Fe oxy(hydr)oxides and Mn oxides could indicate that oxidizing agents (i.e. O_2, nitrate, Fe oxy(hydr)oxides and Mn oxides) were replenished in the sediments at that point due to incidental mixing. In both instances, higher PO_4-Mn and Mn-AEC suggest that Mn, which did not escape from the sediments through reductive dissolution, was trapped mainly in Mn carbonates and some phosphates, resulting in increased Mn/Fe ratios in periods of persisting anoxia.

S-Fe that consists mainly of pyrite and S-Mn (F6), is also considered to have formed endogenically, yet only in small quantities in our record. Sulfides like pyrite are formed in completely reduced sediments where both reductive dissolution of ferric oxides and reduction of sulfate takes place (Håkanson and Jansson, 1983; Holmer and Storkholm, 2001; Luther et al., 2003). These conditions seem to prevail in unit I (Oldest Dryas) and in unit IV around 250 cal BP (Figs. 3B and 5). In the Oldest Dryas (unit I), S-Fe contributes to higher Fe accumulation in the sediments together with the residual Fe and the crystalline Fe oxy(hydr)oxides mentioned before. Consequently, the XRF-Mn/Fe ratio is low in a period of well oxygenated water column (Makri et al., 2020, Fig. 5). However, S-Fe formation and very low Mn concentration suggest the presence of reducing conditions in the sediments in this period, reported also in other lakes (Lake Steisslingen; Eusterhues et al., 2002; Lake Burgäschisee; Rey et al., 2017; Lake Cadagno; Wirth et al., 2013). At the same time, it seems that enhanced detrital input increased the availability of reactive iron (ferrous iron) in the sediments, which allowed S-Fe to be formed. This is also confirmed by the correlation of F6 with Ti (Fig. 4). Similar observations have been made in Lake Cadagno, where little S-Fe was formed in the organic rich layers due to Fe^{2+} limitation, and more S-Fe formed in the silty and sandy layers (Losher, 1989; Wirth et al., 2013). Around 250 cal BP (unit IV), the XRF-Mn/Fe ratio decreases, whereas Bphe is absent and the proportion of Mn-oxides is higher in the sediments. Nonetheless, S-Fe formation again indicates endogenic formation in reducing sediments. An elevated S content, possibly combined with higher detrital material providing adequate reactive iron, could be used as a tracer of intensive diagenetic processes and S-Fe formation.

Humic Mn and humic Fe (F3) are formed endogenously in oxygenated surface waters rich in humic and fulvic acids. Depending on the availability of dissolved humic substances, both Mn and Fe form organometallic structures with dissolved organic matter that can be very stable under anoxic conditions (Lalonde et al., 2012; Paludan and Jensen, 1995). This process is mostly evident during the meromictic phase from ca. 5550 to 5100 cal BP in unit III (Fig. 5). Around 5200 cal BP, both humic Fe and Mn peak. Higher humic and fulvic acids in the sediments are indicated by higher TOC/TN ratios (>10), which suggests terrestrial sources of organic matter rich in humic compounds (Figs. 3 and 5). Increased productivity and soil development in the catchment (Makri et al., 2020) increased the input of allogenic organic carbon into the lake and thus humic matter available for metal complexing. Around 5200 cal BP, when humic Mn peaks, the XRF-Mn/Fe ratio shows an increase, which suggests oxic conditions, whereas Bphe remains high, suggesting persisting anoxia (Fig. 5). The formation of humic Fe and Mn complexes is more likely under higher humic matter content in the lake. C/N ratios higher than 10 indicate increased contributions of terrestrial organic matter (Meyers, 2003) rich in humic and fulvic acids, which can increase the Fe and Mn pool in the sediments.

Iron and manganese partitioning in Lake Moossee and the comparison with the Bphe record (Makri et al., 2020) indicate that the XRF-Mn/Fe ratio is more likely to reflect hypolimnetic redox conditions at times of holomixis with minor effects from detrital, diagenetic or humic matter interactions. In Lake Moossee, this is the case mainly between 14,300 and 5500 cal BP, and in phases between 2000 cal BP to present (Fig. 5), when Fe oxy(hydr)oxides and Mn oxides proportions are dominant (Fig. 3A). The importance of regular bottom water oxygenation for a successful application of the Mn/Fe ratio has also been emphasized in other studies (Loizeau et al., 2001; Naeher et al., 2013; Żarczyński et al., 2019). The application of the Mn/Fe ratio proxy can be limited during periods of higher detrital input or during phases of pronounced or permanent anoxia when diagenetic processes in the sediments prevail (Fig. 5). Diagenetic and detrital input alteration of the Mn/Fe ratio have also been reported in other studies (Friedrich et al., 2014; Hongve, 1997; Naeher et al., 2013; Poraj-Górska et al., 2017; Rothe et al., 2014).

5. Conclusions

Fe and Mn speciation analysis of Lake Moossee over the last 15,000 years provided indications of specific processes that can alter Fe and Mn accumulation and their ratios in the sediments.

The XRF-Mn/Fe ratio successfully reflects paleoredox conditions at times when redox processes governed Fe and Mn accumulation under regular bottom water oxygenation. However, Fe and Mn accumulation and the elemental ratio was influenced by processes other than redox conditions during times of high detrital inputs, prolonged hypolimnetic anoxia, development of anoxic sediments and intensive diagenetic processes, and/or higher DOC input. During times of highly reducing sediments and pronounced or permanent hypolimnetic anoxia, the precipitation and diagenetic formation of AEC-Mn, PO_4-Mn, and humic Mn affected Mn mobility and net loss from the sediments. Consequently, the XRF-Mn/Fe ratio appears higher and cannot be used effectively as a proxy for anoxia. At times of higher erosional input into the lake, Fe and Mn accumulation was governed by detrital sources of residual and crystalline Fe oxy(hydr)oxides and Mn oxides, masking any effect of redox processes. The XRF-Mn/Fe ratio showed lower values during these times of good bottom water oxygenation and regular mixing.

This study has shown that short and long-term changes in bottom water oxygenation governed by prolonged seasonal stratification or insufficient mixing can affect Fe and Mn accumulation in the sediments considerably. These effects can limit the use of these metals and their ratios as exclusive redox proxies. Thus, the use of the XRF-Mn/Fe ratio alone can be inadequate to infer past redox conditions. Multi proxy approaches that combine diverse biogeochemical indicators should be used instead, in order to understand and take into account the environmental conditions and processes affecting the accumulation of Fe and Mn. Further work at subvarve scale combining μXRF with HSI imaging techniques may elucidate in detail the biogeochemical processes and enable fine-scale tracing of redox changes.

CRediT authorship contribution statement

Stamatina Makri: Investigation, Data curation, Formal analysis, Writing - original draft, Visualization. **Giulia Wienhues:** Investigation, Writing - review & editing. **Moritz Bigalke:** Validation, Resources, Writing - review & editing. **Adrian Gilli:** Investigation, Writing - review & editing. **Fabian Rey:** Validation, Data curation. **Willy Tinner:** Conceptualization, Methodology. **Hendrik Vogel:** Investigation, Writing - review

& editing. **Martin Grosjean:** Conceptualization, Methodology, Writing - review & editing, Supervision, Funding acquisition.

Declaration of competing interest

The authors declare that they have no known competing financial interests or personal relationships that could have appeared to influence the work reported in this paper.

Acknowledgments

This study was funded by the Hans-Sigrist-Stiftung and the Swiss National Science Foundation Grants (SNF 200021_172586). SM and MG designed this study and prepared the manuscript. GW performed the analytical laboratory work and SM the data analysis. All co-authors commented on the manuscript. We owe special thanks to Daniela Fischer and Patrick Neuhaus for their assistance in the lab. We also thank Simon Milligan and Paul Zander for English revision, and Bernd Zolitschka and an anonymous reviewer for their constructive and thoughtful comments.

Data availability

The data are available in BORIS at https://boris.unibe.ch/id/eprint/148053.

Appendix A. Supplementary data

Supplementary data to this article can be found online at https://doi.org/10.1016/j.scitotenv.2020.143418.

References

Adekola, F.A., Abdus-Salam, N., Bale, R.B., Oladeji, I.O., 2010. Sequential extraction of trace metals and particle size distribution studies of Kainji Lake sediment, Nigeria. Chem. Speciat. Bioavailab. 22, 43–49. https://doi.org/10.3184/095422910X12631427911623.

Berner, R.A., 1981. A new geochemical classification of sedimentary environments. J. Sediment. Res. 51, 359–365. https://doi.org/10.1306/212F7C7F-2B24-11D7-8648000102C1865D.

Bortleson, G., Lee, G., 1974. Phosphorus, iron, and manganese distribution in sediment cores of six Wisconsin lakes. Limnol. Oceanogr. 19, 794–801. https://doi.org/10.4319/lo.1974.19.5.0794.

Boyle, J.F., 2001. Inorganic geochemical methods in palaeolimnology. Developments in paleoenvironmental research. In: Last, W.M., Smol, J.P. (Eds.), Tracking Environmental Change Using Lake Sediments. Kluwer Academic Publishers, Dordrecht, pp. 83–141 https://doi.org/10.1007/0-306-47670-3_5.

Brandt, M.J., Johnson, K.M., Elphinston, A.J., Ratnayaka, D.D., 2017. Chemistry, microbiology and biology of water. In: Malcolm, J.B., Michael, J.K., Elphinston, A.J., Ratnayaka, D.D. (Eds.), Twort's Water Supply. Butterworth-Heinemann, pp. 235–321 https://doi.org/10.1016/b978-0-08-100025-0.00007-7.

Cornell, R.M., Schwertmann, U., 2003. The Iron Oxides: Structure, Properties, Reactions, Occurences and Uses, Second Edition. 2nd ed. Wiley-VCH Verlag GmbH & Co. KGaA, Weinheim https://doi.org/10.1002/3527602097.

Davison, W., 1993. Iron and manganese in lakes. Earth Sci. Rev. 34, 119–163. https://doi.org/10.1016/0012-8252(93)90029-7.

Dean, W., 2002. A 1500-year record of climatic and environmental change in Elk Lake, Clearwater County, Minnesota II: geochemistry, mineralogy, and stable isotopes. J. Paleolimnol. 27, 301–319. https://doi.org/10.1023/A:1016054522905.

Dhir, B., 2018. Biotechnological tools for remediation of acid mine drainage (removal of metals from wastewater and leachate). Bio-geotechnologies for Mine Site Rehabilitation. Elsevier, pp. 67–82 https://doi.org/10.1016/B978-0-12-812986-9.00004-X.

Engstrom, D., Swain, E., Kingston, J., 2006. A palaeolimnological record of human disturbance from Harvey's Lake, Vermont: geochemistry, pigments and diatoms. Freshw. Biol. 15, 261–288. https://doi.org/10.1111/j.1365-2427.1985.tb00200.x.

Eusterhues, K., Lechterbeck, J., Schneider, J., Wolf-Brozio, U., 2002. Late- and Post-Glacial evolution of Lake Steisslingen (l).: sedimentary history, palynological record and inorganic geochemical indicators. Palaeogeogr. Palaeoclimatol. Palaeoecol. 187, 341–371. https://doi.org/10.1016/S0031-0182(02)00486-8.

Fang, X., Stefan, H.G., 2009. Simulations of climate effects on water temperature, dissolved oxygen, and ice and snow covers in lakes of the contiguous United States under past and future climate scenarios. Limnol. Oceanogr. https://doi.org/10.4319/lo.2009.54.6_part_2.2359.

Foley, B., Jones, I.D., Maberly, S.C., Rippey, B., 2012. Long-term changes in oxygen depletion in a small temperate lake: effects of climate change and eutrophication. Freshw. Biol. https://doi.org/10.1111/j.1365-2427.2011.02662.x.

Friedrich, J., Janssen, F., Aleynik, D., Bange, H.W., Boltacheva, N., Çagatay, M.N., Dale, A.W., Etiope, G., Erdem, Z., Geraga, M., Gilli, A., Gomoiu, M.T., Hall, P.O.J.J., Hansson, D., He, Y., Holtappels, M., Kirf, M.K., Kononets, M., Konovalov, S., Lichtschlag, A., Livingstone, D.M., Marinaro, G., Mazlumyan, S., Naeher, S., North, R.P., Papatheodorou, G., Pfannkuche, O., Prien, R., Rehder, G., Schubert, C.J., Soltwedel, T., Sommer, S., Stahl, H., Stanev, E.V., Teaca, A., Tengberg, A., Waldmann, C., Wehrli, B., Wenzhöfer, F., 2014. Investigating hypoxia in aquatic environments: diverse approaches to addressing a complex phenomenon. Biogeosciences 11, 1215–1259. https://doi.org/10.5194/bg-11-1215-2014.

Gächter, R., Müller, B., 2003. Why the phosphorus retention of lakes does not necessarily depend on the oxygen supply to their sediment surface. Limnol. Oceanogr. 48, 929–933. https://doi.org/10.4319/lo.2003.48.2.0929.

Geoportal des Kantons Bern, 2019. Direktion für Inn. und Justiz Amt für Geoinf. URL. https://www.geo.apps.be.ch/de/. (Accessed 22 December 2019) (WWW Document).

Gu, S., Qian, Y., Jiao, Y., Li, Q., Pinay, G., Gruau, G., 2016. An innovative approach for sequential extraction of phosphorus in sediments: ferrous iron P as an independent P fraction. Water Res. https://doi.org/10.1016/j.watres.2016.07.058.

Guthruf, J., Guthruf-Seiler, K., Zeh, M., 1999. Petits plans d'eau du canton de Berne. Bern.

Guthruf, K., Maurer, V., Rico, R., Zeh, M., Zweifel, N., 2015. Zustand der Kleinseen 2013. Bern.

Håkanson, L., Jansson, M., 1983. Principles of Lake Sedimentology, Principles of Lake Sedimentology. Springer-Verlag, Berlin, New York https://doi.org/10.1007/978-3-642-69274-1.

Hall, G.E.M., Pelchat, P., 1997. Comparison of two reagents, sodium pyrophosphate and sodium hydroxide, in the extraction of labile metal organic complexes. Water, Air, and Soil Pollution https://doi.org/10.1023/A:1018317407840.

Hall, G.E.M., Vaive, J.E., Beer, R., Hoashi, M., 1996. Selective leaches revisited, with emphasis on the amorphous Fe oxyhydroxide phase extraction. J. Geochem. Explor. 56, 59–78. https://doi.org/10.1016/0375-6742(95)00050-X.

Hamilton-Taylor, J., Davison, W., 1995. Redox-driven cycling of trace elements in lakes. In: Lerman, A., Imboden, D., Gat, J. (Eds.), Physics and Chemistry of Lakes. Springer, Berlin Heidelberg, pp. 217–263 https://doi.org/10.1007/978-3-642-85132-2_8.

Harb, C., 2017. Moosseedorf, Moossee Ein Überblick über 160 Jahre Pfahlbauforschung.

Heiri, O., Lotter, A.F., Lemcke, G., 2001. Loss on ignition as a method for estimating organic and carbonate content in sediments: reproducibility and comparability of results. J. Paleolimnol. 25, 101–110.

Holmer, M., Storkholm, P., 2001. Sulphate reduction and sulphur cycling in lake sediments: a review. Freshw. Biol. 46, 431–451. https://doi.org/10.1046/j.1365-2427.2001.00687.x.

Hongve, D., 1997. Cycling of iron, manganese, and phosphate in a meromictic lake. Limnol. Oceanogr. 42, 635–647. https://doi.org/10.4319/lo.1997.42.4.0635.

Imboden, D.M., 1998. The influence of biogeochemical processes on the physics of lakes. Physical Processes in Lakes and Oceans. American Geophysical Union (AGU), pp. 591–612 https://doi.org/10.1029/CE054p0591.

Imhoff, J.F., 2014. The family Chromatiaceae. In: Rosenberg, E., DeLong, E.F., Lory, S., Stackebrandt, E., Thompson, F. (Eds.), The Prokaryotes: Gammaproteobacteria. Springer Berlin Heidelberg, Berlin, Heidelberg, pp. 151–178 https://doi.org/10.1007/978-3-642-38922-1_295.

Jenny, J.-P., Arnaud, F., Dorioz, J.-M., Covex, C.G., Frossard, V., Sabatier, P., Millet, L., Reyss, J.-L., Tachikawa, K., Bard, E., Pignol, C., Soufi, F., Romeyer, O., Perga, M.-E., 2013. A spatiotemporal investigation of varved sediments highlights the dynamics of hypolimnetic hypoxia in a large hard-water lake over the last 150 years. Limnol. Oceanogr. 58, 1395–1408. https://doi.org/10.4319/lo.2013.58.4.1395.

Koinig, K.A., Shotyk, W., Lotter, A.F., Ohlendorf, C., Sturm, M., 2003. 9000 years of geochemical evolution of lithogenic major and trace elements in the sediment of an alpine lake - the role of climate, vegetation, and land-use history. J. Paleolimnol. 30, 307–320.

Kylander, M.E., Ampel, L., Wohlfarth, B., Veres, D., 2011. High-resolution X-ray fluorescence core scanning analysis of Les Echets (France) sedimentary sequence: new insights from chemical proxies. J. Quat. Sci. 26, 109–117.

Lalonde, K., Mucci, A., Ouellet, A., Gelinas, Y., 2012. Preservation of organic matter in sediments promoted by iron. Nature 483, 198–200. https://doi.org/10.1038/nature10855.

Larner, B.L., Palmer, A.S., Seen, A.J., Townsend, A.T., 2008. A comparison of an optimised sequential extraction procedure and dilute acid leaching of elements in anoxic sediments, including the effects of oxidation on sediment metal partitioning. Anal. Chim. Acta 608, 147–157. https://doi.org/10.1016/j.aca.2007.12.016.

Lazzaretti, M.A., Hanselmann, K.W., Brandl, H., Span, D., Bachofen, R., 1992. The role of sediments in the phosphorus cycle in Lake Lugano. II. Seasonal and spatial variability of microbiological processes at the sediment-water interface. Aquat. Sci. 54, 285–299. https://doi.org/10.1007/BF00878142.

Loizeau, J.L., Span, D., Coppee, V., Dominik, J., 2001. Evolution of the trophic state of Lake Annecy (eastern France) since the last glaciation as indicated by iron, manganese and phosphorus speciation. J. Paleolimnol. 25, 205–214. https://doi.org/10.1023/A:1008100432461.

Losher, A., 1989. The Sulfur Cycle in Freshwater Lake Sediments and Implications for the Use of C/S Ratios as Indicators of Past Environmental Changes. ETH Zürich https://doi.org/10.3929/ETHZ-A-000569398.

Luther, G.W., Glazer, B., Ma, S., Trouwborst, R., Shultz, B.R., Druschel, G., Kraiya, C., 2003. Iron and sulfur chemistry in a stratified lake: evidence for Iron-rich sulfide complexes. Aquat. Geochem. 9, 87–110. https://doi.org/10.1023/B:AQUA.0000019466.62564.94.

Mackereth, F.J.H., 1966. Some chemical observations on post-glacial lake sediments. Philos. Trans. R. Soc. Lond. Ser. B Biol. Sci. 250, 165–213. https://doi.org/10.1098/rstb.1966.0001.

Makri, S., Rey, F., Gobet, E., Gilli, A., Tinner, W., Grosjean, M., 2020. Early human impact in a 15,000-year high-resolution hyperspectral imaging record of paleoproduction and

anoxia from a varved lake in Switzerland. Quat. Sci. Rev. 239, 106335. https://doi.org/10.1016/j.quascirev.2020.106335.
Martynova, M.V., 2010. Iron compound occurrence forms in freshwater deposits: analytical review. Water Resour. 37, 488–496. https://doi.org/10.1134/S0097807810040081.
MeteoSwiss, 2019. Evolution annuelle température/ensoleillement précipitations. URL. https://www.meteosuisse.admin.ch/home/climat/climat-de-la-suisse/evolution-annuelle-temperature-ensoleillement-precipitations.html. (Accessed 18 November 2019) (WWW Document).
Meyers, P.A., 2003. Applications of organic geochemistry to paleolimnological reconstructions: a summary of examples from the Laurentian Great Lakes. Organic Geochemistry. Pergamon, pp. 261–289 https://doi.org/10.1016/S0146-6380(02)00168-7.
Munsell Color (Firm), 2010. Munsell Soil Color Charts: With Genuine Munsell Color Chips. 2009 Year Revised. Grand Rapids, MI: Munsell Color, 2010.
Naeher, S., Smittenberg, R.H., Gilli, A., Kirilova, E.P., Lotter, A.F., Schubert, C.J., 2012. Impact of recent lake eutrophication on microbial community changes as revealed by high resolution lipid biomarkers in Rotsee (Switzerland). Org. Geochem. 49, 86–95. https://doi.org/10.1016/j.orggeochem.2012.05.014.
Naeher, S., Gilli, A., North, R.P., Hamann, Y., Schubert, C.J., 2013. Tracing bottom water oxygenation with sedimentary Mn/Fe ratios in Lake Zurich, Switzerland. Chem. Geol. 352, 125–133. https://doi.org/10.1016/j.chemgeo.2013.06.006.
Nriagu, J.O., 1972. Stability of vivianite and ion-pair formation in the system fe3(PO4)2-H3PO4H3PO4-H2o. Geochim. Cosmochim. Acta 36, 459–470. https://doi.org/10.1016/0016-7037(72)90035-X.
Nriagu, J.O., Dell, C.I., 1974. Diagenetic formation of iron phosphates in recent lake sediments. Am. Mineral. 59, 934–946.
Nürnberg, G.K., 1995. Quantifying anoxia in lakes. Limnol. Oceanogr. https://doi.org/10.4319/lo.1995.40.6.1100.
Nurnberg, G.K., Dillon, P.J., 1993. Iron budgets in temperate lakes. Can. J. Fish. Aquat. Sci. 50, 1728–1737. https://doi.org/10.1139/f93-194.
Paludan, C., Jensen, H.S., 1995. Sequential extraction of phosphorus in freshwater wetland and lake sediment: significance of humic acids. Wetlands 15, 365–373. https://doi.org/10.1007/BF03160891.
Peltier, E., Dahl, A.L., Gaillard, J.-F., 2005. Metal speciation in anoxic sediments: when sulfides can be construed as oxides. Environ. Sci. Technol. 39, 311–316. https://doi.org/10.1021/es049212c.
Poraj-Górska, A.I., Żarczyński, M.J., Ahrens, A., Enters, D., Weisbrodt, D., Tylmann, W., 2017. Impact of historical land use changes on lacustrine sedimentation recorded in varved sediments of Lake Jaczno, northeastern Poland. Catena 153, 182–193. https://doi.org/10.1016/j.catena.2017.02.007.
R Core Team, 2015. R: A Language and Environment for Statistical Computing.
Rapin, F., Tessier, A., Campbell, P.G.C., Carignan, R., 1986. Potential artifacts in the determination of metal partitioning in sediments by a sequential extraction procedure. Environ. Sci. Technol. 20, 836–840. https://doi.org/10.1021/es00150a014.
Rey, F., Gobet, E., van Leeuwen, J.F.N., Gilli, A., van Raden, U.J., Hafner, A., Wey, O., Rhiner, J., Schmocker, D., Zünd, J., Tinner, W., 2017. Vegetational and agricultural dynamics at Burgäschisee (Swiss Plateau) recorded for 18,700 years by multi-proxy evidence from partly varved sediments. Veg. Hist. Archaeobot. 26, 571–586. https://doi.org/10.1007/s00334-017-0635-x.
Rey, F., Gobet, E., Schwörer, C., Wey, O., Hafner, A., Tinner, W., 2019a. Causes and mechanisms of synchronous succession trajectories in primeval Central European mixed Fagus sylvatica forests. J. Ecol. 107, 1392–1408. https://doi.org/10.1111/1365-2745.13121.
Rey, F., Gobet, E., Szidat, S., Lotter, A.F., Gilli, A., Hafner, A., Tinner, W., 2019b. Radiocarbon wiggle matching on laminated sediments delivers high-precision chronologies. Radiocarbon 61, 265–285. https://doi.org/10.1017/RDC.2018.47.
Rey, F., Gobet, E., Schwörer, C., Hafner, A., Szidat, S., Tinner, W., 2020. Climate impacts on vegetation and fire dynamics since the last deglaciation at Moossee (Switzerland). Clim. Past 16, 1347–1367. https://doi.org/10.5194/cp-16-1347-2020.
Rothe, M., Frederichs, T., Eder, M., Kleeberg, A., Hupfer, M., 2014. Evidence for vivianite formation and its contribution to long-term phosphorus retention in a recent lake sediment: a novel analytical approach. Biogeosciences 11, 5169–5180. https://doi.org/10.5194/bg-11-5169-2014.
Schaller, T., Wehrli, B., 1996. Geochemical-focusing of manganese in lake sediments - an indicator of deep-water oxygen conditions. Aquat. Geochem. 2, 359–378. https://doi.org/10.1007/BF00115977.
Schindler, D.W., 2006. Recent advances in the understanding and management of eutrophication. Limnol. Oceanogr. 51, 356–363. https://doi.org/10.4319/lo.2006.51.1_part_2.0356.
Schmid, S.M., Fügenschuh, B., Kissling, E., Schuster, R., 2004. Tectonic map and overall architecture of the Alpine orogen. Eclogae Geol. Helv. 97, 93–117. https://doi.org/10.1007/s00015-004-1113-x.
Shaw, P.J., 1994. The effect of pH, dissolved humic substances, and ionic composition on the transfer of iron and phosphate to particulate size fractions in epilimnetic lake water. Limnol. Oceanogr. https://doi.org/10.4319/lo.1994.39.7.1734.
Sobczyński, T., Siepak, J., 2001. Speciation of heavy metals in bottom sediments of lakes in the area of Wielkopolski National Park. Polish J. Environ. Stud. 10, 463–474.
Stevens, L., Ito, E., Olson, D., 2000. Relationship of Mn-carbonates in varved lake-sediments to catchment vegetation in Big Watab Lake, MN, USA. J. Paleolimnol. 24, 199–211. https://doi.org/10.1023/A:1008169526577.
Templeton, D.M., Ariese, F., Cornelis, R., Danielsson, L.G., Muntau, H., Van Leeuwen, H.P., Łobiński, R., 2000. Guidelines for terms related to chemical speciation and fractionation of elements. Definitions, structural aspects, and methodological approaches (IUPAC recommendations 2000). Pure Appl. Chem. https://doi.org/10.1351/pac200072081453.
Tipping, E., Jones, J.G., Woof, C., 1985. Lacustrine manganese oxides: Mn oxidation states and relationships to "Mn depositing bacteria". Arch. Hydrobiol. 161–175.
Tonolla, M., Peduzzi, S., Hahn, D., Peduzzi, R., 2003. Spatio-temporal distribution of phototrophic sulfur bacteria in the chemocline of meromictic Lake Cadagno (Switzerland). FEMS Microbiol. Ecol. 43, 89–98. https://doi.org/10.1016/S0168-6496(02)00354-9.
Tribovillard, N., Algeo, T.J., Lyons, T., Riboulleau, A., 2006. Trace metals as paleoredox and paleoproductivity proxies: an update. Chem. Geol. 232, 12–32. https://doi.org/10.1016/j.chemgeo.2006.02.012.
United Nations, 2015. Transforming our World: The 2030 Agenda for Sustainable Development. Geneva.
van der Zee, C., Roberts, D.R., Rancourt, D.G., Slomp, C.P., 2003. Nanogoethite is the dominant reactive oxyhydroxide phase in lake and marine sediments. Geology 31, 993–996. https://doi.org/10.1130/G19924.1.
Vegas-Vilarrúbia, T., Corella, J.P., Pérez-Zanón, N., Buchaca, T., Trapote, M.C., López, P., Sigró, J., Rull, V., 2018. Historical shifts in oxygenation regime as recorded in the laminated sediments of lake Montcortès (Central Pyrenees) support hypoxia as a continental-scale phenomenon. Sci. Total Environ. 612, 1577–1592. https://doi.org/10.1016/j.scitotenv.2017.08.148.
Vuillemin, A., Friese, A., Wirth, R.A., Schuessler, J.M., Schleicher, A., Kemnitz, H., Lücke, A.W., Bauer, K., Nomosatryo, S., Von Blanckenburg, F., Simister, R.G., Ordoñez, L., Ariztegui, D., Henny, C.M., Russell, J., Bijaksana, S., Vogel, H.A., Crowe, S., Kallmeyer, J., 2020. Vivianite formation in ferruginous sediments from Lake Towuti, Indonesia. Biogeosciences 17, 1955–1973. https://doi.org/10.5194/bg-17-1955-2020.
Wersin, P., Höhener, P., Giovanoli, R., Stumm, W., 1991. Early diagenetic influences on iron transformations in a freshwater lake sediment. Chem. Geol. https://doi.org/10.1016/0009-2541(91)90102-W.
Wetzel, R.G., 2001. Limnology: lake and river ecosystems. 3rd ed Journal of Phycology. Acedemic Press.
White, J.R., Gubala, C.P., 1990. Sequentially extracted metals in Adirondack lake sediment cores. J. Paleolimnol. 3, 243–252. https://doi.org/10.1007/BF00219460.
Wirth, S.B., Gilli, A., Niemann, H., Dahl, T.W., Ravasi, D., Sax, N., Hamann, Y., Peduzzi, R., Peduzzi, S., Tonolla, M., Lehmann, M.F., Anselmetti, F.S., 2013. Combining sedimentological, trace metal (Mn, Mo) and molecular evidence for reconstructing past water-column redox conditions: the example of meromictic Lake Cadagno (Swiss Alps). Geochim. Cosmochim. Acta 120, 220–238. https://doi.org/10.1016/j.gca.2013.06.017.
Woolway, R.I., Merchant, C.J., 2019. Worldwide alteration of lake mixing regimes in response to climate change. Nat. Geosci. 12, 271–276. https://doi.org/10.1038/s41561-019-0322-x.
Żarczyński, M., Wacnik, A., Tylmann, W., 2019. Tracing lake mixing and oxygenation regime using the Fe/Mn ratio in varved sediments: 2000 year-long record of human-induced changes from Lake Żabińskie (NE Poland). Sci. Total Environ. 657, 585–596. https://doi.org/10.1016/J.SCITOTENV.2018.12.078.